Hindawi
Journal of Nanomaterials
Volume 2017, Article ID 7214617, 9 pages
https://doi.org/10.1155/2017/7214617

Research Article

Preparation of Cerium Dioxide Layers on Titanium by Electrodeposition with Organic Solution

Vaijayanti Namdeo Nande, Diana Kostyukova, Jeonghee Choi, and Yong Hee Chung

Department of Chemistry, Hallym University, 1 Hallymdaehak-gil, Chuncheon 24252, Republic of Korea

Correspondence should be addressed to Yong Hee Chung; yhchung@hallym.ac.kr

Received 31 January 2017; Accepted 20 April 2017; Published 15 May 2017

Academic Editor: Flavio Colmati

Layers of cerium dioxide nanoparticles were prepared on titanium by electrodeposition with organic solution. Three concentrations of cerium ions were used at 31.6 V. The organic solution was isobutanol and titanium foils were used as anodes and cathodes. Currents were monitored during the electrodeposition. Deposition times ranged from 0.5 to 8 h. Deposited Deposited layers were calcined at 700 K for 30 min. The morphology and composition of the deposited layers were examined by scanning electron microscopy (SEM), X-ray diffraction (XRD), and X-ray photoelectron spectroscopy (XPS). As-prepared and calcined deposition layers were assayed to be cerium dioxide. The average crystallite size increased from 4 to 7 nm through calcination at 700 K. Sizes of calcined cerium oxide agglomerates were ranging from 73 to 146 nm for 30 min deposition and 209 to 262 nm for 8 h deposition. The electrodeposition efficiencies of 0.5 h deposition at three concentrations were measured to be highest.

1. Introduction

Targets of cerium dioxide with thicknesses in range of several mg/cm^2 were used in proton-induced nuclear reactions [1–3]. Cerium dioxide was deposited on aluminum. Targets of cerium dioxide with a thickness in range of mg/cm^2 deposited on titanium can be used to verify cross sections of production of ^{142}Pr whose values were reported to disagree at proton energies in the vicinity of 12 MeV [1, 2]. Titanium has been used to precisely monitor the proton energy up to 30–40 MeV using the ^{nat}Ti(p,xn)^{48}V nuclear reaction [4–6].

Thin layers of cerium dioxide (CeO_2) have been prepared by various methods such as electrodeposition [7–9], hydrothermal [10], ion beam-assisted deposition [11], laser chemical vapor deposition [12–14], microwave-assisted heating [15], precipitation [16, 17], magnetron sputtering [18, 19], and sol–gel [20] methods. CeO_2 has salient characteristics such as oxygen buffer layers, high dielectric constant, and distinctive photocatalytic and optical properties, which allows its diverse applications in direct methanol fuel cells [21–23], direct alcohol fuel cells [24], proton exchange membrane (PEM) fuel cells [25, 26], solid oxide fuel cells [27], and solar cells [28], humidity and chemical sensors [29–31], dye-degradation [32], and sunscreen cosmetics [33]. Cerium oxide with a cubic fluorite structure in the reduced state has two charge states of Ce^{3+} and Ce^{4+}, resulting in oxygen vacancies which contribute to large oxygen storage capacity [34, 35]. Properties of nanocrystalline CeO_2 were reported to be different from those of microcrystalline counterpart in ionic conductivity and chemical reactivity [36].

In this work nanocrystalline CeO_2 layers of various thicknesses were prepared on titanium by electrodeposition in isobutanol of three concentrations of Ce^{3+} ions at 31.6 V, similarly to nanocrystalline lanthanum oxide and lanthanum oxycarbonate layers prepared at much higher voltages ranging from 200 to 1000 V [37]. Three concentrations of Ce^{3+} ions used in the electrodeposition were 0.046, 0.092, and 2.0 mg/mL and currents were monitored during the electrodeposition. Deposition times ranged from 0.5 to 8 h. The as-prepared layers were then calcined at 700 K for 30 min. The morphology and composition of the deposition layers were examined by scanning electron microscopy (SEM), X-ray diffraction (XRD), and X-ray photoelectron spectroscopy (XPS). Effects of electrodeposition concentration and time

on morphology of calcined layers and electrodeposition efficiency were investigated. Concurrently, structural data for as-prepared and calcined layers of nanocrystalline CeO_2 were deduced.

2. Experimental Details

Cerium nitrate hexahydrate ($Ce(NO_3)_3{\cdot}6H_2O$, ≥99.0%, Fluka) powder was dissolved in a minimal amount of distilled water and further in isobutanol. The aqueous-organic mixture was evaporated by heating above 94°C to its nearly dried state, whose composition was examined by X-ray photoelectron spectroscopy (XPS, Thermo Scientific K-Alpha$^+$ spectrometer) with an Al Kα microfocused monochromator. The dried cerium nitrate precursor was dissolved in isobutanol and the resulting solutions with concentrations of Ce^{3+} ions of 0.046, 0.092, and 2.0 mg/mL, corresponding to 0.33, 0.66, and 14.5 mM, respectively, were used in the electrodeposition.

The electrodeposition was carried out at room temperature in a cell which was made of Teflon and used in the previous study [37]. The electrodeposition area was 3.14 cm^2 and the distance between the electrodes was 10 mm. The cell was filled up to 3.5 mL with the organic cerium nitrate solution. Polished titanium foils were used as anodes and cathodes whose typical thickness was 11.4 μm. The titanium electrodes were washed consecutively by nitric acid, distilled water, and ethanol before being assembled into the cell. Voltage of the electrodeposition performed at room temperature was 31.6 V. The electrodeposition times of each concentration were 0.5, 2, 4, 6, and 8 h. The currents were monitored during the deposition time. Layers of deposited cerium oxide were washed consecutively by distilled water and ethanol. After being washed they were kept in ethanol for 24 h in order to remove the residual nitrate electrolyte and dried for 12 h in a drying oven at 50°C. The electrodeposited layers were calcined at 700 K for 30 min. Figure 1 shows the steps involved for syntheses of CeO_2 layers.

Morphology and surface compositions of electrodeposition layers were examined by scanning electron microscopy (SEM, Hitachi S-4300) and X-ray photoelectron spectroscopy (XPS, Thermo Scientific K-Alpha). Their corresponding compositions and structural data with average crystalline sizes were determined from measurements by X-ray diffraction (XRD, PANalytical X'pert PRO MPD) with wavelength of Cu K_α, 1.5405 Å.

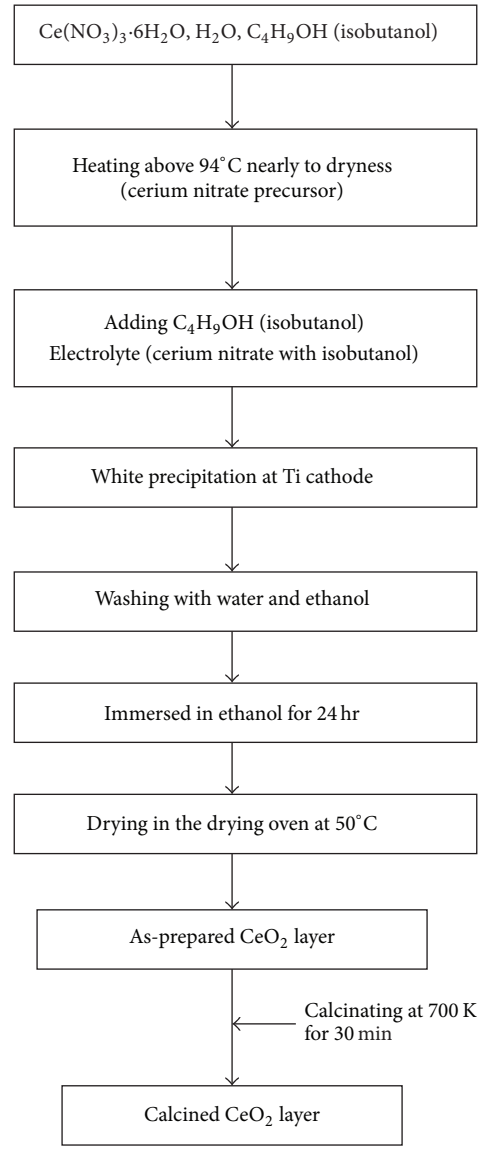

Figure 1: Chart for syntheses of as-prepared and calcined CeO_2 layers.

3. Results and Discussion

XPS spectrum of the cerium nitrate precursor with isobutanol dried on a Ti foil is shown in Figure 2(a). XPS spectra of electrodeposited layers are shown in Figures 2(b) and 2(c) which were obtained as prepared and calcined at 700 K for 30 min, respectively. Figure 2(a) shows photoelectron peaks of bulk Ce 3d, 4p, and 4d, O 1s, N 1s, and C 1s along with Ti 2p arising from a titanium foil. The N 1s, O 1s, and C 1s peaks were due mainly to nitrate and isobutanol. Any significant impurities were not found in the cerium nitrate precursor. Figures 2(b) and 2(c) show photoelectron peaks of Ce 3d, 4p, and 4d, O 1s, and C 1s and their corresponding elemental compositions are listed in Table 1. As shown in Figures 2(b) and 2(c) and Table 1, the carbon and oxygen contents in the layers decreased after calcination.

The Ce $3d_{5/2}$ and $3d_{3/2}$ peaks with their corresponding satellite peaks in Figure 2 are expanded over the binding energy range of 925–875 eV in Figure 3. The Ce $3d_{5/2}$ main peaks for the cerium nitrate precursor and two layers in Figure 3 are at 882.9, 882.8, and 882.8 eV, respectively, while their corresponding $3d_{3/2}$ peaks are at 900.2, 901.3, and 901.2 eV, respectively. The Ce 3d peaks for the layers in Figures 3(b) and 3(c) match well within 0.1 eV, implying that they have the same chemical composition regardless of the calcination. The separation between Ce $3d_{5/2}$ and $3d_{3/2}$ peaks in the layers with or without calcination is 18.4–18.5 eV and the corresponding separation in the cerium nitrate precursor

Table 1: Elemental composition (atomic %) obtained from XPS spectra for cerium nitrate precursor and electrodeposition layers.

Major element* (atomic %)	Cerium nitrate precursor	Layers	
		As-prepared	Calcined at 700 K for 30 min
Ce	4.6	13.0	16.9
O	61.9	52.6	58.8
C	20.3	32.3	24.3
N	13.2	2.1	

*Titanium excluded in elemental compositions.

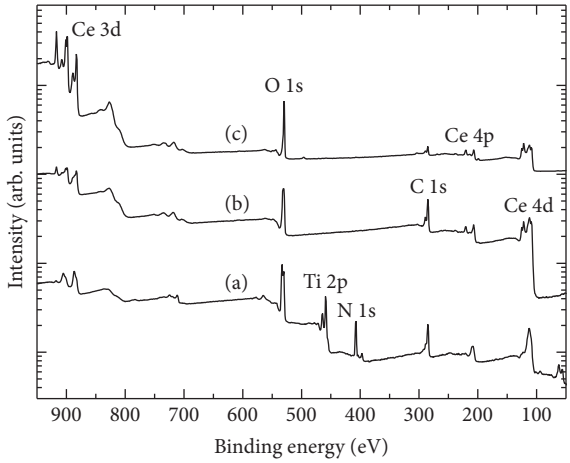

Figure 2: XPS spectra of (a) cerium nitrate precursor dried on Ti and layers on Ti electrodeposited at 31.6 V (b) as prepared and (c) calcined at 700 K for 30 min.

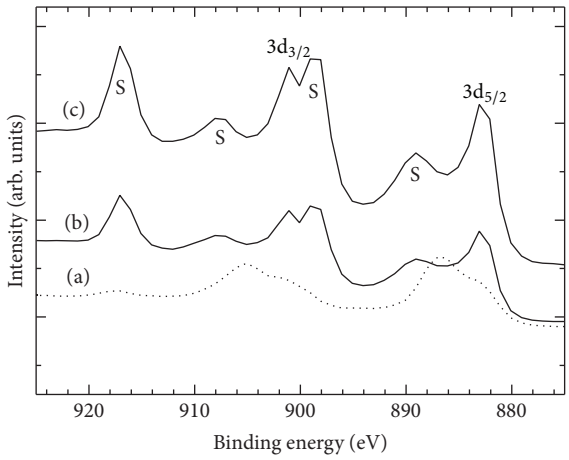

Figure 3: XPS spectra of Ce 3d peaks with their satellite lines denoted as S for (a) cerium nitrate precursor and the layers (b) as prepared and (c) calcined at 700 K for 30 min in Figure 2.

is 17.3 eV. The Ce 3d satellite peaks for the calcined layer are located at 888.0 and 898.4 eV for Ce $3d_{5/2}$ and at 906.4 and 916.9 eV for $3d_{3/2}$, while those for the as-prepared layer appear at 887.7 and 898.5 eV for Ce $3d_{5/2}$ and at 905.8 and 917.0 eV for $3d_{3/2}$. They agree well within 0.1–0.6 eV. The broad Ce 3d peaks of the cerium nitrate precursor in Figure 3(a) reveal its bulk properties.

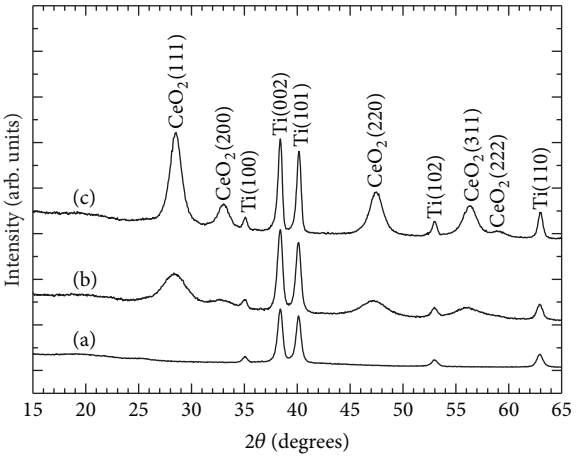

Figure 4: X-ray diffraction patterns of (a) cerium nitrate precursor dried on Ti and electrodeposition layers on Ti (b) as prepared and (c) calcined at 700 K for 30 min.

A wide-angle X-ray diffraction (XRD) pattern of the cerium nitrate precursor with isobutanol dried on a Ti foil is shown in Figure 4(a). XRD patterns of electrodeposition layers are shown in Figures 4(b) and 4(c), which were obtained as prepared and calcined at 700 K for 30 min, respectively. Figures 4(a)–4(c) show hexagonal Ti with crystal faces of (100), (002), (101), (102), and (110) due to Ti cathode foils. The as-prepared layer in Figure 4(b) shows diffraction peaks at $2\theta = 28.4^\circ$, 32.8°, 47.2°, and 56.3°, which amount to (111), (200), (220), and (311) reflections of the cubic structure of CeO_2 (JCPDS card number 34-0394). The calcined layer in Figure 4(c) shows diffraction peaks at $2\theta = 28.5^\circ$, 33.0°, 47.4°, 56.3°, and 59.2°, which amount to (111), (200), (220), (311), and (222) reflections of the cubic CeO_2. There are no traces of diffraction peaks of Ce_2O_3 in Figures 4(b) and 4(c), implying that the nanoparticles in the as-prepared and calcined layers were mainly CeO_2. The average crystallite size was estimated using Scherrer equation [17, 20, 37–39]:

$$D = \frac{K\lambda}{\beta \cos\theta}, \quad (1)$$

where D is the average crystallite size, K is the dimensionless shape factor whose typical value is about 0.9, λ is the X-ray wavelength used in XRD (Cu K_α = 1.5405 Å), β is the broadening of the observed diffraction line at half the maximum intensity in radians, and θ is the Bragg angle. The average crystallite sizes of the as-prepared and calcined layers

Table 2: Estimated crystallite size (Scherrer size), lattice parameter a, dislocation density δ, strain, stacking fault (SF), and texture coefficient (TC) of two CeO_2 samples electrodeposited on Ti which were as prepared and calcined at 700 K for 30 min.

CeO_2 sample	hkl	Scherrer size (nm)	a (Å)	δ (nm^{-2})	Strain	SF	TC
As-prepared	111	3.630	5.441	0.07587	0.00955	0.01983	1.1899
	200	4.146	5.439	0.05817	0.00836	0.01628	0.8344
	220	4.049	5.451	0.06098	0.00856	0.01432	1.1136
	311	3.175	5.424	0.09918	0.01092	0.01714	0.8622
Calcined at 700 K for 30 min	111	6.991	5.428	0.02046	0.00496	0.01029	1.1364
	200	8.494	5.426	0.01386	0.00408	0.00792	0.9499
	220	6.572	5.420	0.02315	0.00527	0.00880	1.0453
	311	6.612	5.420	0.02287	0.00524	0.00823	0.8685

were estimated using (1) and concurrently structural data such as lattice parameter, dislocation density, strain, stacking fault, and texture coefficient were estimated and listed in Table 2.

The average crystallite sizes of the as-prepared CeO_2 layer in Table 2 were deduced from (111), (200), (220), and (311) reflections at $2\theta = 28.4^\circ$, 32.8°, 47.2°, and 56.3°, respectively, while those of the calcined layer were deduced from its corresponding reflections at $2\theta = 28.5^\circ$, 33.0°, 47.4°, and 56.3°. The additional structural parameters such as lattice parameter a, dislocation density δ, strain ε, stacking fault (SF), and texture coefficient (TC) were estimated using the following relations [17, 39]:

$$
\begin{aligned}
a &= \frac{n\lambda}{2\sin\theta}\sqrt{h^2 + k^2 + l^2}, \\
\delta &= \frac{1}{D^2}, \\
\varepsilon &= \frac{\beta\cos\theta}{4}, \\
\mathrm{SF} &= \frac{2\pi^2\beta}{45\sqrt{3\tan\theta}}, \\
\mathrm{TC} &= \frac{I_o(h_i k_i l_i)}{I_s(h_i k_i l_i)}\left[\frac{1}{N}\sum_{i=1}\frac{I_o(h_i k_i l_i)}{I_s(h_i k_i l_i)}\right]^{-1},
\end{aligned}
\tag{2}
$$

where λ is the X-ray wavelength used in XRD (Cu K_α = 1.5405 Å), β is the broadening of the observed diffraction line at half the maximum intensity in radians, θ is the Bragg angle, D is the average crystallite size, $h_i k_i l_i$s are Miller indices, N is the number of diffraction peaks, and I_o and I_s are observed and sample intensities, respectively. Table 2 shows that the average crystalline size for the (111) crystal face increased from 3.63 to 6.99 nm through the 30 min calcination process at 700 K, while the corresponding lattice parameter decreased from 5.441 to 5.428 Å. The dislocation density δ for the (111) face was reduced from 0.07587 to 0.02046 nm^{-2} and its corresponding microstrain decreased from 0.00955 to 0.00496. Consequently the stacking fault for the (111) face was reduced from 0.01983 to 0.01029 even though the corresponding texture coefficient decreased only by about 4.5%.

SEM micrographs of CeO_2 layers obtained by 0.5 or 8 h electrodeposition with 0.046, 0.092, and 2.0 mg/mL of Ce^{3+} ions and subsequent 30 min calcination at 700 K are shown in Figure 5. The CeO_2 layers of the 30 min electrodeposition in Figures 5(a), 5(c), and 5(e) contain agglomerates with sizes ranging from 7 to 73, 7 to 94, and 7 to 146 nm, respectively, indicating that the sizes of agglomerates increase as the concentration of Ce^{3+} ions increases. At the 8 h electrodepositions in Figures 5(b), 5(d), and 5(f), the sizes of agglomerates increase to 209, 251, and 262 nm, respectively. The sizes of calcined CeO_2 agglomerates increased at higher concentrations and longer electrodeposition times even though the typical sizes of the corresponding as-prepared CeO_2 particles were measured from their SEM data to be in the vicinity of 4 nm regardless of the concentration and deposition time.

Currents of 0.5, 2, 4, 6, and 8 h electrodepositions at 31.6 V with 0.046, 0.092, and 2.0 mg/mL of Ce^{3+} ions are shown in Figures 6–10, respectively. Figure 6 shows that the currents of 0.5 h electrodepositions at 0.046, 0.092, and 2.0 mg/mL increase from 27 to 50, 32 to 62, and 356 to 643 μA, respectively. In Figure 7, the currents of 2 h electrodepositions at 0.046 and 0.092 mg/mL increase from 26 to 90 and 51 to 132 μA, respectively, while the corresponding currents at 2.0 mg/mL increase gradually from 367 to 768 μA for 65 min and slowly to 783 μA for 30 min and slowly decrease to 741 μA. In Figure 8, the currents of 4 h electrodepositions at 0.046 and 0.092 mg/mL increase with minor variations from 53 to 133 and 58 to 144 μA, respectively, while the corresponding currents at 2.0 mg/mL increase gradually from 388 to 739 μA for 45 min, decrease slowly to 645 μA for 75 min, increase sharply to 803 μA for 5 min, and then decrease slowly to 613 μA with some fluctuations. In Figure 9, the currents of 6 h electrodeposition at 0.046 mg/mL increase from 60 to 109 μA for 260 min and slowly decrease to 88 μA with minor variations, and those at 0.092 mg/mL slowly increase from 64 to 90 μA for 160 min, then increase sharply to 208 μA and drop to 176 μA for 5 min, and decrease slowly to 161 μA, while those at 2.0 mg/mL increase sharply from 303 to 467 μA for 25 min, decrease to 409 μA for 20 min, then increase to 468 μA after 20 min, decrease gradually to 319 μA for 65 min, and remain steady. Figure 10 shows that the currents of 8 h electrodepositions at 0.046, 0.092, and 2.0 mg/mL increase with minor variations from 68 to 127, 110 to 250, and 272 to

Table 3: Thicknesses and yields of electrodepositions for three concentrations of Ce^{3+} ions.

Deposition time (h)	Concentration of Ce^{3+} ions (mg/mL)					
	0.046		0.092		2.0	
	Thickness (mg/cm^2)	Yield (%)	Thickness (mg/cm^2)	Yield (%)	Thickness (mg/cm^2)	Yield (%)
0.5	0.015 ± 0.014	24 ± 22	0.021 ± 0.015	17 ± 12	0.16 ± 0.02	5.7 ± 0.9
2	0.057 ± 0.010	91 ± 16	0.050 ± 0.014	40 ± 11	0.40 ± 0.04	15 ± 1
4	0.067 ± 0.015	106 ± 25	0.090 ± 0.019	72 ± 15	0.43 ± 0.03	16 ± 1
6	0.054 ± 0.022	86 ± 35	0.099 ± 0.018	78 ± 15	0.42 ± 0.03	15 ± 1
8	0.067 ± 0.062	106 ± 40	0.150 ± 0.036	120 ± 29	0.35 ± 0.03	13 ± 1

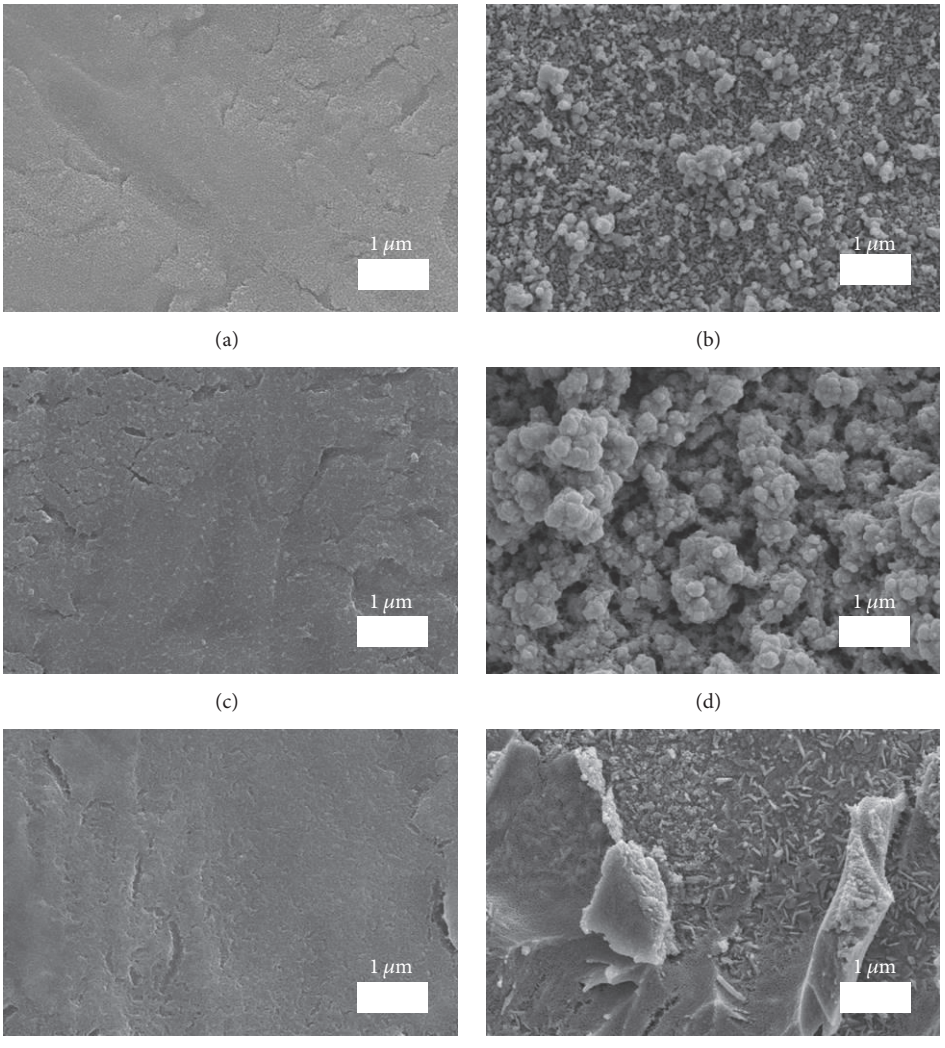

Figure 5: SEM micrographs of CeO_2 layers calcined at 700 K for 30 min after (a) 30 min electrodeposition of 0.046 mg/mL of Ce^{3+} on Ti, (b) 8 h electrodeposition of 0.046 mg/mL of Ce^{3+}, (c) 30 min electrodeposition of 0.092 mg/mL of Ce^{3+}, (d) 8 h electrodeposition of 0.092 mg/mL of Ce^{3+}, (e) 30 min electrodeposition of 2.0 mg/mL of Ce^{3+}, and (f) 8 h electrodeposition of 2.0 mg/mL of Ce^{3+}.

314 μA, respectively. The higher concentrations of Ce^{3+} ions induced the higher currents due to the increase of cerium ions.

Thicknesses and yields of 0.5, 2, 4, 6, and 8 h electrodepositions at 31.6 V with 0.046, 0.092, and 2.0 mg/mL of Ce^{3+} ions are shown in Figures 11–13 and Table 3, respectively. The yields of 0.5, 2, and 4 h electrodepositions at 0.046 mg/mL in Figure 11 are ~24, ~91, and ≥100%, respectively. Their corresponding thicknesses were 0.015, 0.057, and 0.067 mg/cm^2, respectively, implying that the deposition efficiency was highest at 0.5 h deposition and sharply decreased after 2 h. The yields of 0.5, 2, 4, 6, and 8 h electrodepositions

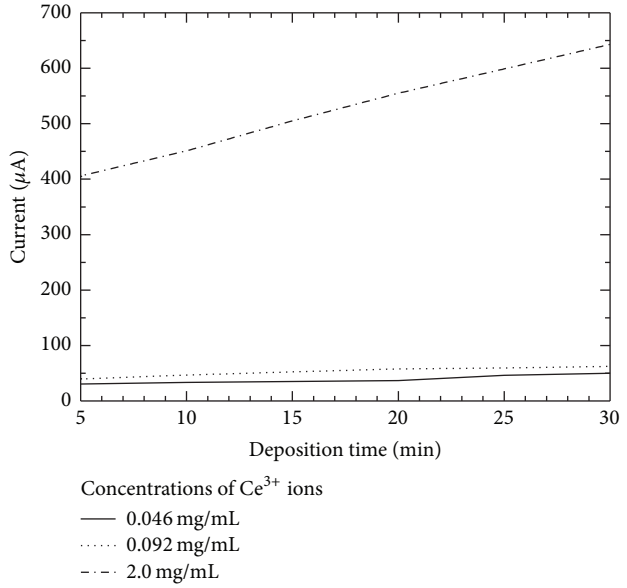

Figure 6: Currents of 0.5 h electrodepositions with three concentrations of Ce^{3+} ions at 31.6 V.

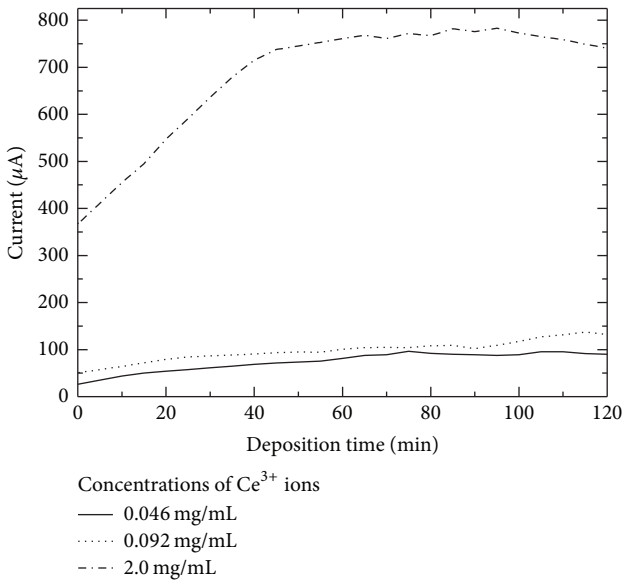

Figure 7: Currents of 2 h electrodepositions with three concentrations of Ce^{3+} ions at 31.6 V.

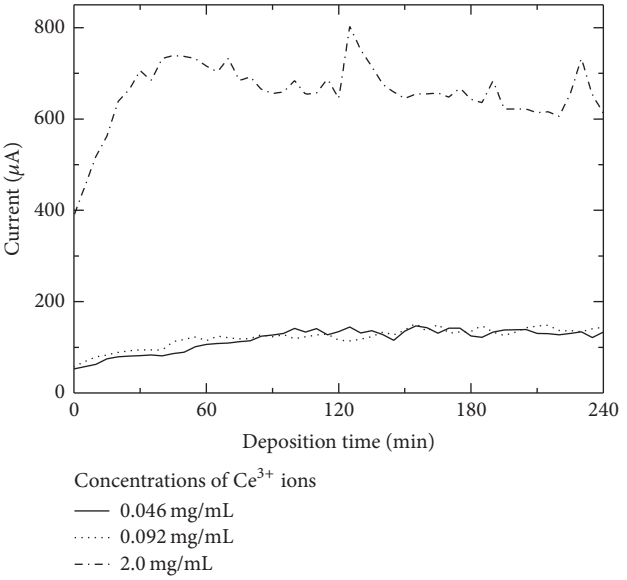

Figure 8: Currents of 4 h electrodepositions with three concentrations of Ce^{3+} ions at 31.6 V.

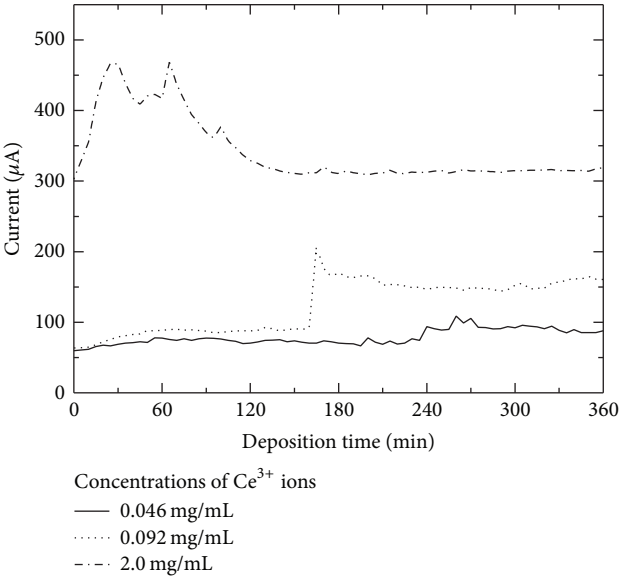

Figure 9: Currents of 6 h electrodepositions with three concentrations of Ce^{3+} ions at 31.6 V.

at 0.092 mg/mL in Figure 12 and Table 3 are 17, 40, 72, 78, and ≥100%, respectively. Their corresponding thicknesses were 0.021, 0.050, 0.090, 0.099, and 0.150 mg/cm^2, respectively, implying that the deposition efficiency was highest at 0.5 h deposition. Figure 13 shows that the yields of 0.5, 2, 4, 6, and 8 h electrodepositions at 2.0 mg/mL are 6, 15, 16, 15, and 13%, respectively. Their corresponding thicknesses were 0.16, 0.40, 0.43, 0.42, and 0.35 mg/cm^2, respectively, implying that the deposition efficiency was highest at 0.5 h electrodeposition as observed at the lower concentrations. The deposition efficiency was highest at 0.5 h deposition at all three concentrations. The 0.5 h electrodeposition at the highest concentration is suitable for preparation of thicker layers of cerium dioxide.

Similar results for XPS and XRD of as-prepared samples were observed irrespective of currents and deposition times. Typical particle sizes of as-prepared and calcined cerium dioxide samples shown in the corresponding SEM data were 4 and 7 nm, respectively, regardless of their concentrations, indicating that nucleation was driven mainly by the applied potential. However, the deposition time affected the size of calcined agglomerates, showing that longer deposition times increase the corresponding sizes.

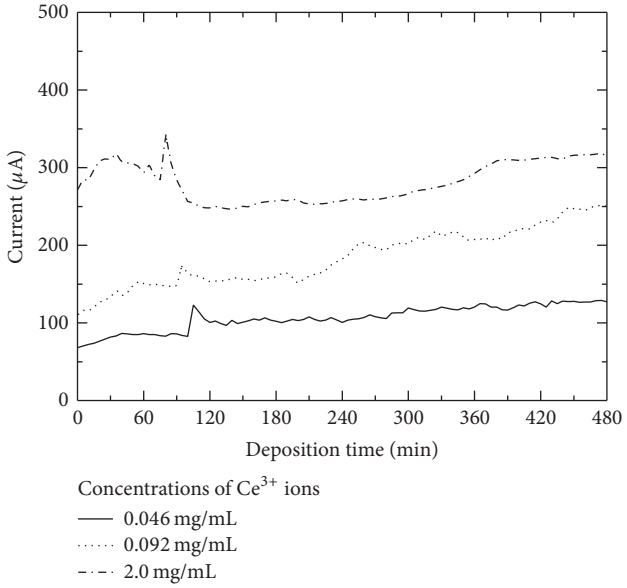

Figure 10: Currents of 8 h electrodepositions with three concentrations of Ce^{3+} ions at 31.6 V.

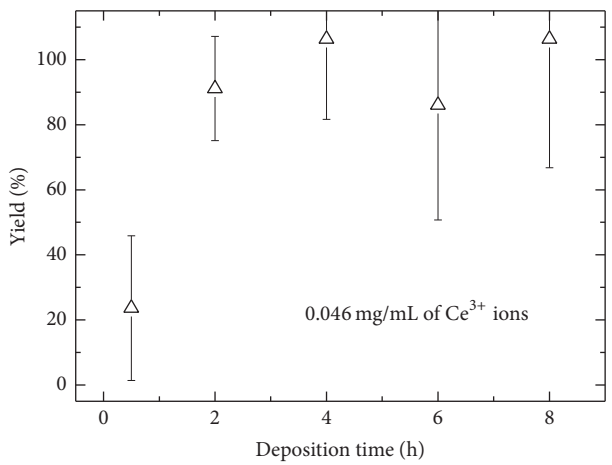

Figure 11: Yields of electrodepositions with 0.046 mg/mL of Ce^{3+} ions at 31.6 V.

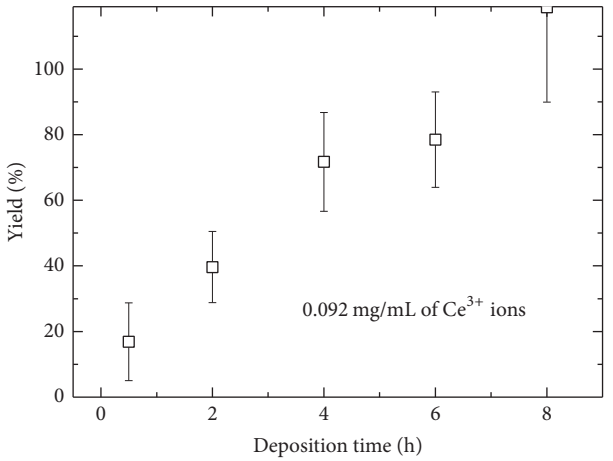

Figure 12: Yields of electrodepositions with 0.092 mg/mL of Ce^{3+} ions at 31.6 V.

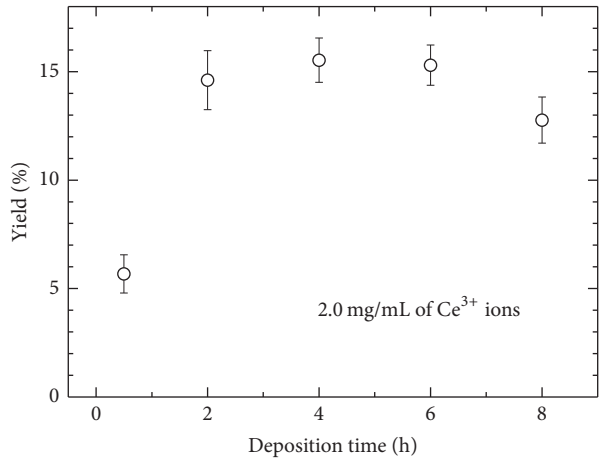

Figure 13: Yields of electrodepositions with 2.0 mg/mL of Ce^{3+} ions at 31.6 V.

4. Conclusions

Layers of CeO_2 nanoparticles with thicknesses ranging from 0.021 to 0.43 mg/cm^2 were prepared on titanium by electrodeposition with isobutanol solution and subsequent calcination. As-prepared and calcined deposited layers turned out to be cubic CeO_2. The average crystallite size increased from 4 to 7 nm through calcination at 700 K for 30 min irrespective of the concentration and the current. Structural parameters such as lattice parameter, dislocation density, strain, and stacking factors were reduced by the calcination. The deposition time affected the size of calcined agglomerates as longer deposition times increased the corresponding sizes.

The electrodeposition efficiency was highest at 0.5 h deposition at all three concentrations. The 0.5 h electrodeposition at the highest concentration is suitable for preparation of thicker layers of cerium dioxide, which are to be used in the investigation of cross sections of ^{142}Pr produced in the proton-induced reaction with cerium.

Conflicts of Interest

The authors declare that they have no conflicts of interest.

Acknowledgments

This work was financially supported by AMIE Fund.

References

[1] M. Furukawa, "Excitation functions for proton-induced reactions of ^{140}Ce and ^{142}Ce up to E_p = 15 MeV," *Nuclear Physics, Section A*, vol. 90, no. 2, pp. 253–260, 1967.

[2] E. V. Verdieck and J. M. Miller, "Radiative capture and neutron emission in $La^{139}+\alpha$ and Ce^{142}+p," *Physical Review*, vol. 153, no. 4, pp. 1253–1261, 1967.

[3] H. G. Blosser and T. H. Handley, "Survey of (p,n) reactions at 12 Mev," *Physical Review*, vol. 100, no. 5, pp. 1340–1344, 1955.

[4] P. Kopecky, F. Szelecsényi, T. Molnár, P. Mikecz, and F. Tárkányi, "Excitation functions of (p, xn) reactions on ^{nat}Ti: monitoring of bombarding proton beams," *Applied Radiation and Isotopes*, vol. 44, no. 4, pp. 687–692, 1993.

[5] M. U. Khandaker, K. Kim, M. W. Lee et al., "Investigations of the ^{nat}Ti(p,x)^{43,44m,44g,46,47,48}Sc, ^{48}V nuclear processes up to 40 MeV," *Applied Radiation and Isotopes*, vol. 67, no. 7-8, pp. 1348–1354, 2009.

[6] A. Hermanne, F. Tárkányi, S. Takács, F. Ditrói, and N. Amjed, "Excitation functions for production of ^{46}Sc by deuteron and proton beams in ^{nat}Ti: A basis for additional monitor reactions," *Nuclear Instruments and Methods in Physics Research, Section B: Beam Interactions with Materials and Atoms*, vol. 338, pp. 31–41, 2014.

[7] P. Stefanov, G. Atanasova, D. Stoychev, and T. Marinova, "Electrochemical deposition of CeO_2 on ZrO_2 and Al_2O_3 thin films formed on stainless steel," *Surface and Coatings Technology*, vol. 180-181, pp. 446–449, 2004.

[8] D. Nikolova, E. Stoyanova, D. Stoychev, P. Stefanov, and T. Marinova, "Anodic behaviour of stainless steel covered with an electrochemically deposited Ce_2O_3-CeO_2 film," *Surface and Coatings Technology*, vol. 201, no. 3-4, pp. 1559–1567, 2006.

[9] L. Yang, X. Pang, G. Fox-Rabinovich, S. Veldhuis, and I. Zhitomirsky, "Electrodeposition of cerium oxide films and composites," *Surface and Coatings Technology*, vol. 206, no. 1, pp. 1–7, 2011.

[10] M. Panahi-Kalamuei, S. Alizadeh, M. Mousavi-Kamazani, and M. Salavati-Niasari, "Synthesis and characterization of CeO_2 nanoparticles via hydrothermal route," *Journal of Industrial and Engineering Chemistry*, vol. 21, pp. 1301–1305, 2015.

[11] J. Wang, R. Fromknecht, and G. Linker, "Preparation of biaxially textured CeO_2 buffer layers by ion beam-assisted deposition," *Surface and Coatings Technology*, vol. 158-159, pp. 548–551, 2002.

[12] P. Zhao, A. Ito, R. Tu, and T. Goto, "High-speed epitaxial growth of (100)-oriented CeO_2 film on r-cut sapphire by laser chemical vapor deposition," *Surface and Coatings Technology*, vol. 205, no. 16, pp. 4079–4082, 2011.

[13] P. Zhao, A. Ito, and T. Goto, "Laser chemical vapor deposition of single-crystalline transparent CeO_2 films," *Surface and Coatings Technology*, vol. 235, pp. 273–276, 2013.

[14] P. Zhao, A. Ito, R. Tu, and T. Goto, "Preparation of highly (100)-oriented CeO_2 films on polycrystalline Al_2O_3 substrates by laser chemical vapor deposition," *Surface and Coatings Technology*, vol. 204, no. 21-22, pp. 3619–3622, 2010.

[15] H. Yang, C. Huang, A. Tang, X. Zhang, and W. Yang, "Microwave-assisted synthesis of ceria nanoparticles," *Materials Research Bulletin*, vol. 40, no. 10, pp. 1690–1695, 2005.

[16] S. A. Hassanzadeh-Tabrizi, M. Mazaheri, M. Aminzare, and S. K. Sadrnezhaad, "Reverse precipitation synthesis and characterization of CeO_2 nanopowder," *Journal of Alloys and Compounds*, vol. 491, no. 1-2, pp. 499–502, 2010.

[17] R. Suresh, V. Ponnuswamy, and R. Mariappan, "Effect of annealing temperature on the microstructural, optical and electrical properties of CeO_2 nanoparticles by chemical precipitation method," *Applied Surface Science*, vol. 273, pp. 457–464, 2013.

[18] I.-W. Park, J. Lin, J. J. Moore et al., "Grain growth and mechanical properties of CeO_2-x films deposited on Si(100) substrates by pulsed dc magnetron sputtering," *Surface and Coatings Technology*, vol. 217, pp. 34–38, 2013.

[19] H.-Y. Lee, S.-I. Kim, Y.-P. Hong, Y.-C. Lee, Y.-H. Park, and K.-H. Ko, "Controlling the texture of CeO_2 films by room temperature RF magnetron sputtering," *Surface and Coatings Technology*, vol. 173, no. 2-3, pp. 224–228, 2003.

[20] M. L. Lavčević, A. Turković, P. Dubček, and S. Bernstorff, "Nanostructured CeO_2 thin films: A SAXS study of the interface between grains and pores," *Thin Solid Films*, vol. 515, no. 14, pp. 5624–5626, 2007.

[21] D.-J. Guo and Z.-H. Jing, "A novel co-precipitation method for preparation of Pt-CeO_2 composites on multi-walled carbon nanotubes for direct methanol fuel cells," *Journal of Power Sources*, vol. 195, no. 12, pp. 3802–3805, 2010.

[22] H. Kunitomo, H. Ishitobi, and N. Nakagawa, "Optimized CeO_2 content of the carbon nanofiber support of PtRu catalyst for direct methanol fuel cells," *Journal of Power Sources*, vol. 297, pp. 400–407, 2015.

[23] C. Feng, T. Takeuchi, M. A. Abdelkareem, T. Tsujiguchi, and N. Nakagawa, "Carbon-CeO_2 composite nanofibers as a promising support for a PtRu anode catalyst in a direct methanol fuel cell," *Journal of Power Sources*, vol. 242, pp. 57–64, 2013.

[24] L. Yu and J. Xi, "CeO_2 nanoparticles improved Pt-based catalysts for direct alcohol fuel cells," *International Journal of Hydrogen Energy*, vol. 37, no. 21, pp. 15938–15947, 2012.

[25] F. Xu, R. Xu, and S. Mu, "Enhanced SO2 and CO poisoning resistance of CeO_2 modified Pt/C catalysts applied in PEM fuel cells," *Electrochimica Acta*, vol. 112, pp. 304–309, 2013.

[26] Z. Wang, H. Tang, H. Zhang et al., "Synthesis of Nafion/CeO_2 hybrid for chemically durable proton exchange membrane of fuel cell," *Journal of Membrane Science*, vol. 421-422, pp. 201–210, 2012.

[27] T. Désaunay, A. Ringuedé, M. Cassir, F. Labat, and C. Adamo, "Modeling basic components of solid oxide fuel cells using density functional theory: Bulk and surface properties of CeO_2," *Surface Science*, vol. 606, no. 3-4, pp. 305–311, 2012.

[28] A. Corma, P. Atienzar, H. García, and J.-Y. Chane-Ching, "Hierarchically mesostructured doped CeO_2 with potential for solar-cell use," *Nature Materials*, vol. 3, no. 6, pp. 394–397, 2004.

[29] W. Xie, B. Liu, S. Xiao et al., "High performance humidity sensors based on CeO_2 nanoparticles," *Sensors and Actuators, B: Chemical*, vol. 215, pp. 125–132, 2015.

[30] D. Zhu, Y. Fu, W. Zang, Y. Zhao, L. Xing, and X. Xue, "Piezo/active humidity sensing of CeO_2/ZnO and SnO_2/ZnO nanoarray nanogenerators with high response and large detecting range," *Sensors and Actuators B*, vol. 205, pp. 12–19, 2014.

[31] A. Umar, R. Kumar, M. S. Akhtar, G. Kumar, and S. H. Kim, "Growth and properties of well-crystalline cerium oxide (CeO_2) nanoflakes for environmental and sensor applications," *Journal of Colloid and Interface Science*, vol. 454, pp. 61–68, 2015.

[32] W. Mingyan, Z. Wei, Z. Dongen et al., "CeO_2 hollow nanospheres decorated reduced graphene oxide composite for efficient photocatalytic dye-degradation," *Materials Letters*, vol. 137, pp. 229–232, 2014.

[33] S. Yabe and T. Sato, "Cerium oxide for sunscreen cosmetics," *Journal of Solid State Chemistry*, vol. 171, no. 1-2, pp. 7–11, 2003.

[34] C. T. Campbell and C. H. F. Peden, "Oxygen vacancies and catalysis on ceria surfaces," *Science*, vol. 309, no. 5735, pp. 713-714, 2005.

[35] K. Wang, Y. Chang, L. Lv, and Y. Long, "Effect of annealing temperature on oxygen vacancy concentrations of nanocrystalline CeO_2 film," *Applied Surface Science*, vol. 351, pp. 164–168, 2015.

[36] I. Kosacki, T. Suzuki, V. Petrovsky, and H. U. Anderson, "Electrical conductivity of nanocrystalline ceria and zirconia thin films," *Solid State Ionics*, vol. 136-137, pp. 1225–1233, 2000.

[37] J. Choi and Y. H. Chung, "Preparation of lanthanum oxide and lanthanum oxycarbonate layers on titanium by electrodeposition with organic solution," *Journal of Nanomaterials*, vol. 2016, pp. 1–13, 2016.

[38] C. Esther Jeyanthi, R. Siddheswaran, R. Medlín, M. Karl Chinnu, R. Jayavel, and K. Rajarajan, "Electrochemical and structural analysis of the RE^{3+}:CeO_2 nanopowders from combustion synthesis," *Journal of Alloys and Compounds*, vol. 614, pp. 118–125, 2014.

[39] J. Malleshappa, H. Nagabhushana, S. C. Sharma et al., "Leucas aspera mediated multifunctional CeO_2 nanoparticles: Structural, photoluminescent, photocatalytic and antibacterial properties," *Spectrochimica Acta - Part A: Molecular and Biomolecular Spectroscopy*, vol. 149, pp. 452–462, 2015.